analytical chemistry

Article

Cite This: Anal. Chem. 2017, 89, 13283−13289

pubs.acs.org/ac

Impedimetric Sensor of ss-HSDNA/Reduced Graphene Oxide Aerogel Electrode toward Aflatoxin B1 Detection: Effects of Redox Mediator Charges and Hydrodynamic Diffusion

Atiweena Krittayavathananon and Montree Sawangphruk*

Department of Chemical and Biomolecular Engineering, School of Energy Science and Technology, Vidyasirimedhi Institute of Science and Technology, Rayong 21210, Thailand

Supporting Information

ABSTRACT: Here, an impedimetric biosensor for determination and quantification of an aflatoxin B1 (AFB1) level using a reduced graphene oxide aerogel labeled with a single strand DNA (ss-HSDNA/rGO_{ae}) modified on a rotating disk electrode (RDE) is presented. Owing to the large biomolecule biding on the electrode, an electron transfer is interrupted and not easily accessible to a target molecule. To address this issue, we aim to study two effects; one considers electro-redox mediators and the other considers the hydrodynamic effect. By observing a cyclic voltammetric response from the ss-HSDNA/rGO_{ae} electrode in three different charges of the redox mediators (i.e., neutral $FcCH_2OH$, cationic $Ru(NH_3)_6^{3+}$, and anionic $Fe(CN)_6^{4-}$) in a phosphate buffer solution (PBS) containing AFB1, the magnitude of anodic current at 50 mV s^{-1} is 825, 615, and 550 mA cm^{-1}, respectively, which is significant dominated by the charge of the redox probe. The effect of hydrodynamic diffusion of the ss-HSDNA/rGO_{ae} rotating disk electrode (RDE) toward AFB1 detection using $FcCH_2OH$ as the redox mediator was recorded by applying a range of rotating speed from 500 to 4000 rpm. Increasing rotating speed reduces the charge transfer resistance resulting in the lower detectable level for AFB1 quantification. In the case of 4000 rpm, the AFB1 can be detected with a limit of detection of 0.04 ng/mL and a linear range of 1×10^{-10} to 7×10^{-8} g/mL.

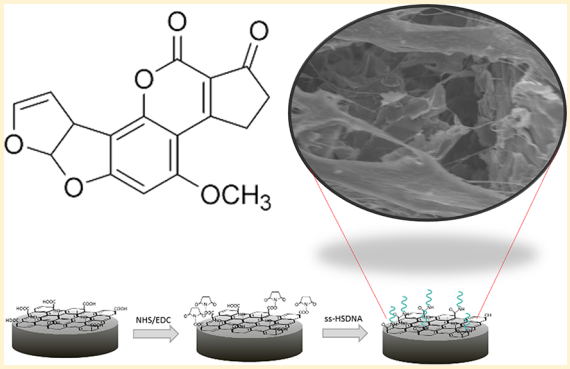

Aflatoxin B1 (AFB1) is one type of aflatoxins that is a group of highly toxic compounds produced by *Aspergillus* species.[1] Among more than 20 aflatoxins species, only four species (B1, B2, G1, and G2) have been classified as human carcinogens. According to International Agency for Research on Cancer (IARC) report, AFB1 is the most toxic agent when compared to other aflatoxins leading to human liver cancer. AFB1 is widely infected in a wide range of agricultural and animal products such as cereals, nuts, peanuts, corn, fruits, and dried fruits during growth and storage.[2,3] Hence, many countries have drawn a regulation of the maximum level of AFB1 that can be contaminated in foodstuffs. The European Commission has set a maximum value of AFB1 at 2 μg/kg.[2] The U.S. Food and Drug Administration (FDA) has limited 20 μg/kg for all aflatoxins in the human food.[3] Also, the aflatoxins in an agricultural product are controlled by ISO/IEC 17025.[4]

Among analytical methods, an electrochemical impedance spectroscopy (EIS) is of interest.[5] Recently, EIS has become a powerful technique for studying biochemical and biophysical processes. As compared with voltammetry, which is normally used to determine aflatoxin B1,[6,7] EIS provides higher sensitivity, resulting in the lower limit of detection of the target molecule. The first successful impedimetric AFB1 sensor was reported by Dinçkaya et al.[8] Single-stranded DNA (ss-DNA) is modified on an electrode surface to recognize its target molecule based on a lock and key process. The sensor monitors the change of the conductive surfaces before and after the target molecule binding on the electrode surface. To improve the sensing performance, recent studies focus on two components, one considers the electrode and the other considers the medium or electrolyte. Properties of electrode materials including high electrical conductivity, high stability, and large surface area play a significant role in the impedance response. Most of these properties are exhibited by graphene; therefore, in the recent year, graphene-based sensors have been a massive explosion with an excellent analytical performance.[9−11]

In term of the electrolyte, a soluble redox mediator is added to the electrolyte which can mediate the efficient transport of electron reducing charge transfer resistances. However, no exact recipe for choosing the redox mediator has been reported. While a group of ferrocyanide ions ($Fe(CN)_6^{4-}$) is applied in many biosensors as observed in the literature (Table S1 in the Supporting Information), Patolsky et al.[12] presented an

Received: August 17, 2017
Accepted: November 24, 2017
Published: November 24, 2017

DOI: 10.1021/acs.analchem.7b03329
Anal. Chem. 2017, 89, 13283−13289

enhancement of electron transfer resistance of a hybridization between liposomes and DNA modified on gold electrode in the hexacyanoferrate solution due to the electrostatic repulsion between negatively charged liposomes and the negative charge of the mediator. According to our previous work,[13] by observing a response from three different charges of the redox mediator (i.e., neutral $FcCH_2OH$, cationic $Ru(NH_3)_6^{3+}$, and anionic $Fe(CN)_6^{4-}$) on a reduced graphene oxide (rGO) electrode, the electrochemical behavior is dependent on the charge of the redox probe. Due to the negative charge of oxygen-containing groups on the rGO surface, the obtained current response in $Fe(CN)_6^{4-}$ solution is far from the theoretical value, which is reasonably relating with the Patolsky et al. work. By contrast, the electrochemical behavior of the rGO electrode is more favorable in the positive molecule $Ru(NH_3)_6^{3+}$, as well as the attractive $\pi-\pi$ interaction between two aromatic cyclopentadienyl rings of neutral $FcCH_2OH$ and benzene rings on the rGO structure plays a significant role. Herein, a single-strand DNA (ss-HSDNA) is modified on the reduced graphene aerogel (rGO_{ae}) electrode. Phosphate groups on the DNA backbone provide a negative charge leading to the increase of negatively charged coverage on the electrode interface.[14] To find a suitable redox mediator, the electrochemical behavior of those modified electrodes is recorded in the three different charges of the redox probe.

Though the use of suitable redox mediators can improve the electron transfer, the detection process becomes limited under ion transport with slow diffusing properties. The simple process to illuminate mass transport is to include the hydrodynamic properties of the system. In the case of electrochemical sensors, the hydrodynamic diffusion is usually observed via a cyclic voltammetry,[15,16] but no report uses the electrochemical impedance spectroscopy (EIS). The efficient technique is to use a rotating disk electrode (RDE) system.[17] As the electrode rotates, the solution is driven by a centripetal force into the center of electrode surface allowing products to diffuse out of the electrode surface and, on the other hand, allowing analytic sample in the solution to diffuse to the electrode surface. The rate of chemical reaction depends on the angular velocity (ω), which relates to the current following both Levich equation and Koutecký–Levich equations.[18,19]

In this work, the AFB1 sensor was fabricated using the ss-HSDNA modified on the rGO_{ae} electrode via a self-immobilization process.[8] The effects of redox-mediated species in the electrolytes and hydrodynamic diffusion were extensively investigated leading to high-performance and more reliable impedimetric biosensor for determination and quantification of an aflatoxin B1. In terms of practical application, the as-developed method is further applied to detect aflatoxin in ultrahigh-temperature (UTH) milk.

EXPERIMENTAL SECTION

Chemicals and Materials. Chemicals used in this work are of analytical grade and used without further purification including graphite powder (20–40 μm, Sigma–Aldrich), sulfuric acid (98.0%, QRec), hydrogen peroxide (30.0%, Merck), potassium permanganate (99.0%, Ajax Finechem), DNA from herring sperm (ss-HSDNA, Sigma–Aldrich), 1-ethyl-3-(3-(dimethylamino)propyl) carbodiimide hydrochloride (98% EDC, Sigma-Aldrich), *n*-hydroxysuccinimide (97% NHS, Sigma-Aldrich), potassium chloride (99.0%, Sigma-Aldrich), sodium nitrate (99.5%, QRec), potassium dihydrogen phosphate (99.5% KH_2PO_4, Volchem), disodium hydrogen orthophosphate dehydrate (99.0% $Na_2HPO_4{\cdot}2H_2O$, UNILAB), sodium chloride (99.5%, CARLO ERBA), aflatoxins B1 from *Aspergillus flavus* (Sigma-Aldrich), aflatoxin B2 (Sigma-Aldrich), aflatoxin G2 (Sigma-Aldrich), ochratoxin (Sigma-Aldrich), and acetone (99.5%, QRec). For solution preparation, the pure water (resistance of >18.2 MΩ cm at 25 °C) was purified by using the Milli-Q system.

Preparation of Reduced Graphene Aerogel (rGO_{ae}). In brief, 50 mg of graphene oxide (GO) synthesized from the Hummer and Offman method[20] with our modification[21] was ultrasonicated in Milli-Q water (80 mL) for 30 min. A total of 0.5 M hydrazine hydrate was added to the GO suspension and sealed in a Teflon-lined autoclave maintained at 80 °C in an oven (SLN, POL-EKO APARATURA) for 72 h, respectively.[22] The autoclave was naturally cooled down to room temperature at a natural cooling rate. The as-synthesized hydrogel was soaked in water for 24 h to remove residual hydrazine. The hydrogel was frozen in liquid nitrogen and placed in a freezing dryer machine (Labconco, 2.5 L benchtop freeze-dry systems) at −50 °C for 2 days. The final product rGO_{ae} was eventually obtained.

Preparation of ss-HSDNA-Tagged Immobilized on a rGO_{ae} Electrode. The modification process of ss-HSDNA molecule on the rGO_{ae} surface provides two steps, as shown in a schematic in Figure 1. A total of 5 μL of rGO_{ae} suspension in

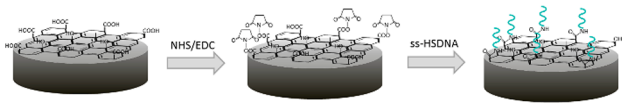

Figure 1. Schematic showing a fabrication process of an ss-HSDNA/rGO_{ae} electrode.

acetone (10 mg/mL) was dropped on a glassy carbon (GC) rotating disk electrode (RDE) with a diameter of 3.0 ± 0.1 mm. Then, the solvent was allowed to evaporate under a N_2 atmosphere. Note that GC RDE was polished with alumina slurry and washed with purified water before use. The first step is a pretreatment process of the rGO_{ae} surface. The functional group on the rGO_{ae} surface was activated with NHS in the presence of EDC used as a cross-linking agent to couple between carboxyl groups and primary amines.[23] The modified electrode was soaked with EDC/NHS solution containing 2 M EDC and 2 M NHS for 2 h at a room temperature. The residual EDC/NHS was then washed by DI solution. The second step is the modification of ss-HSDNA on the electrode surface. The electrode was soaked in 1:16000 of ss-HSDNA in PBS (pH 7.4) for 24 h at 4 °C before washing the unbound ss-HSDNA by Milli-Q water.

Structural and Morphological Characterization. The morphology of the as-prepared material was characterized using Scanning Electron Microscopy (SEM), JSM35CF operated at 20 keV. The chemical structure of rGO_{ae} was evaluated by X-ray photoelectron spectroscopy (XPS) and Fourier transform infrared spectroscopy (FTIR). The XPS technique was employed by AXIS Ultra DLD (Kratos Analytical Ltd., Manchester, U.K.) using Mg-Ka nonmonochromatic radiation (1253.6 eV, 200 W) as an X-ray excitation source. FTIR spectra were recorded by PerkinElmer Paragon 1000. In addition, energy dispersive X-ray spectroscopy (EDX) was used to confirm the element analysis of the as-prepared electrodes.

Electrochemical Evaluation of Aflatoxin B1 Detection. The as-fabricated electrode was used as an electrochemical

DOI: 10.1021/acs.analchem.7b03329
Anal. Chem. 2017, 89, 13283–13289

sensor electrode for detecting AFB1. The electrochemical process with a three-electrode system using the as-fabricated electrode as a working electrode, a platinum wire as a counter current, and a silver−silver chloride (Ag/AgCl) electrode as a reference electrode was set up. The cyclic voltammetry (CV) and electrochemical impedance spectroscopy (EIS) methods were used to evaluate the electrode performance under an ambient temperature (25 °C) using a computer-controlled μ-AUTOLAB II potentiostat (Eco-Chemie, Utrecht, The Netherlands) equipped with a FRA2 frequency response analyzer module running NOVA 1.11 software. All electrolytes in this work were used in a phosphate buffered saline (PBS) at pH 7.4 as an auxiliary electrolyte.

The EIS results are fitted by an equivalent Randles circuit, $R_s(C[R_{ct}Z_w])$, where C is a double-layer capacitance, Z_w is a Warburg impedance, R_s is a solution resistance, and R_{ct} is an electron transfer resistance. Note that R_{ct} is sensitive to species that can perturb the sensing interface. It is a combination of a sensing layer (R_{sens}) and an analyte binding (R_{anal}) that could be written as $R_{ct} = R_{GC} + R_{rGO} + R_{ss\text{-}HSDNA} + R_{AFB1}$.[24]

RESULTS AND DISCUSSION

Physical Characterization. SEM images in Figure 2a (high magnification) and Figure S1 (low magnification) show rGO_{ae}

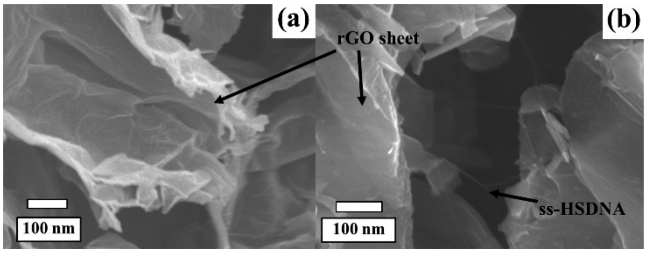

Figure 2. SEM images of (a) rGO_{ae} and (b) ss-HSDNA/rGO_{ae}.

with interconnected graphene sheets producing a framework structure. By using a self-immobilization process,[8] a morphology of ss-DNA modified on the rGO_{ae} surface (ss-HSDNA/rGO_{ae}) is shown in Figure 1b. The presence of ss-HSDNA/rGO_{ae} is a clear evidence indicating the successful immobilization of these biomolecules.

The FTIR and XPS techniques were also carried out to confirm the hybridization process between ss-HSDNA and rGO_{ae}. The FTIR spectrum of the as-prepared rGO_{ae} (in Figure 3a and the enlarged image in Figure S2) displays some residual oxygen functional groups on the rGO_{ae} surface such as hydroxyl (3435 cm^{-1}), carbonyl (1731 cm^{-1}), and epoxy (1042 cm^{-1}).[25] The modification process of ss-HSDNA molecule on the rGO_{ae} surface includes two steps, as shown in a schematic in the Experimental Section. In the first step, the functional group on the rGO_{ae} surface was activated with NHS in the presence of EDC, which is used as a cross-linking agent to couple between carboxyl groups and primary amines. The FTIR spectrum of NHS/rGO_{ae} is shown in Figure S3 in the Supporting Information. On the NHS/rGO_{ae} spectrum, the peak of the NHS ester (1783 and 1814 cm^{-1}) was almost disappeared and turned to Amide II (1552 cm^{-1}), and Amide I (1632 cm^{-1})[26] functionalized on the rGO_{ae} surface. In the second step, NHS/rGO_{ae} was further hybridized with ss-HSDNA (see more details in the Experimental Section). A FTIR spectrum of ss-HSDNA/rGO_{ae} is shown in Figure 3 as compared with pure rGO_{ae} and

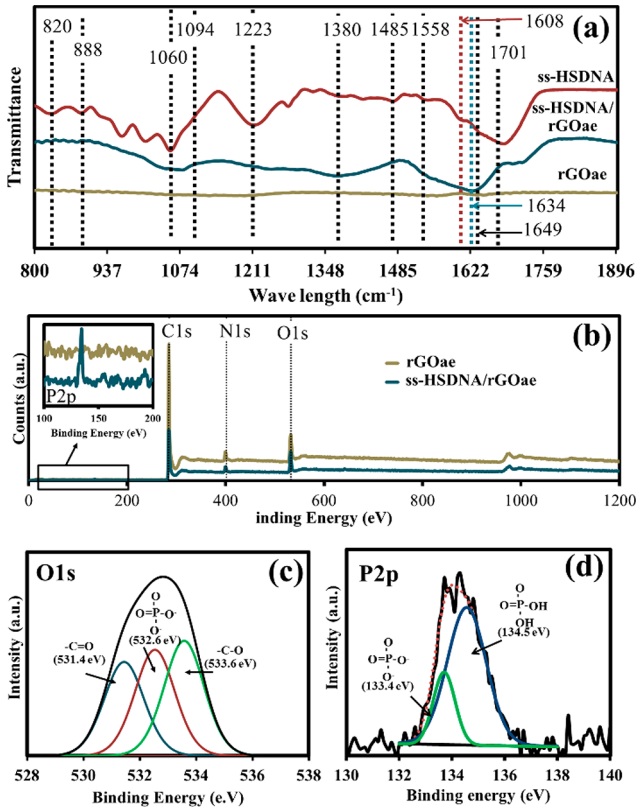

Figure 3. (a) FTIR, (b) wide-scan XPS spectra of ss-HSDNA, ss-HSDNA/rGO_{ae}, and rGO_{ae}, and (c, d) C 1s and P 2p XPS spectra of ss-HSDNA/rGO_{ae}, respectively.

ss-HSDNA spectra. Note that the FTIR spectrum of ss-HSDNA has a similar main peak position with previous reports.[27,28] After rGO_{ae} immobilized with ss-HSDNA, there are many peaks that are dominated by ss-HSDNA such as 1060, 1094, 1223 cm^{-1} corresponding to C−O, symmetric and asymmetric PO_2^- groups on the DNA backbone. The mode at 1485, 1608, 1649, and 1701 cm^{-1} results from DNA bases of purine (adenine and guanine) and pyrimidine (cytosine, thymine), respectively, while Amide II, and Amide I bending vibrations are slightly shift to 1558, and 1634 cm^{-1}, respectively. This observation is also a good evidence for the functionalization of ss-HSDNA.

XPS survey spectra (Figure 3b) present the elements of rGO_{ae} and ss-HSDNA/rGO. It can be seen from the survey spectra that the expected elements C, O, N, and P present on the surface of ss-HSDNA/rGO with a percentage of 82.91, 11.48, 5.41, and 0.19, respectively. The P peak does not appear on the surface of pure rGO_{ae}. Furthermore, Figure 2c,d shows the detailed region of O 1s and P 2p on the ss-HSDNA/rGO_{ae} surface. The O 1s peak contains three subpeaks including carboxyl (-C═O, 531.4 eV), hydroxyl (-C−OH, 533.6 eV), and phosphate (532.6 eV) in the modified biomolecule.[29] The P 2p profile is a strong confirmation of the bond formation between DNA molecule and the rGO_{ae} surface.

Electrochemical Evolution. First, the comparison of ss-HSDNA modified via adsorption (without NHS) and covalent bonding interaction using NHS as a cross-linking agent on the rGO_{ae} surface was carried out (section 4 in the Supporting Information). The result shows that the covalently modified ss-HSDNA on the NHS/rGO_{ae} can enhance the R_{ct} value when compared with the one modified via the adsorption on the

DOI: 10.1021/acs.analchem.7b03329
Anal. Chem. 2017, 89, 13283−13289

rGO_{ae} without using the NHS. The modified ss-HSDNA electrode was placed in phosphate buffer solution (PBS, pH 7.4) containing 2 ng/mL aflatoxin B1 (AFB1) and 6 mM ferrocenemethanol ($FcCH_2OH$) as a redox mediator. The electrochemical response is recorded via a cyclic voltammetry method under a static condition. Figure 4 shows the response

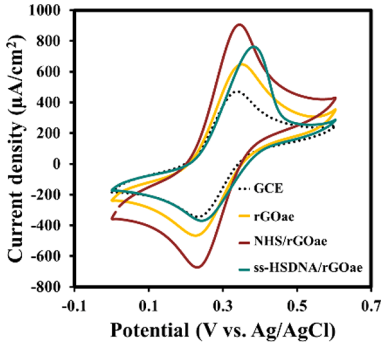

Figure 4. Cyclic voltammograms of GCE, rGO_{ae}, NHS/rGO_{ae}, and ss-HSDNA/rGO_{ae} at 50 mV s^{-1} in PBS (pH 7.4) containing 2 ng/mL AFB1 and 6 mM $FcCH_2OH$.

from a sequence-modified GC electrode following rGO_{ae}/GCE, NHS/rGO_{ae}/GCE, and ss-HSDNA/rGO_{ae}/GCE, respectively. The cyclic voltammograms show a well-defined reversible redox behavior of an electron transfer process between $FcCH_2OH$ and its oxidized form, $FcCH_2OH^+$. The magnitude of the current of NHS/rGO_{ae} is 1.4-fold higher than that of the pure rGO_{ae} and its peak position is shifted to lower peak-to-peak separation, indicating the higher electron transfer kinetics. This is dominated by the nitrogen atom in the amide group of NHS providing different electronegativities between the doping molecule and the carbon adjusting the electroneutrality of carbon and inducing the redistribution of charge transfer state in the molecule.[30] After grafting ss-HSDNA, the magnitude of current decreases when compared with the NHS/rGO_{ae} electrode due to the covalent binding between −CO and −NH,[31,32] which partly blocks the electron transfer exchanging between the liquid/solid interfaces of the $FcCH_2OH$ solution and the electrode surface.

Effect of Redox Mediators. As the sensing mechanism based on the electrochemical communication of the electrode and redox mediator before and after AFB1 binds to ss-HSDNA, the effect of redox mediators is worth being investigated. Three different redox mediators with different charges including neutral $FcCH_2OH$, cationic hexaammineruthenium(III) chloride ($Ru(NH_3)_6^{3+}$), and anionic ferrocyanide ($Fe(CN)_6^{4-}$) were used in this work. A cyclic voltammetric response of the as-fabricated electrode (ss-HSDNA/rGO_{ae}) is placed in the PBS solution containing 2 ng/mL AFB1 and a 6 mM redox mediator. All experiments were carried out under a static condition at various scan rates as shown in Figure 5a–c. Like the current response from the case of $FcCH_2OH$ (Figure 4), the electrochemical redox reaction behavior occurs under the quasi-reversible reaction with one electron transfer process. The redox reaction of the as-prepared material in the $FcCH_2OH$ solution gives higher feedback current than $Ru(NH_3)_6^{3+}$ and $Fe(CN)_6^{4-}$. The oxidation current response of those species was plotted as a function of $(\text{scan rate})^{-1/2}$ (see Figure 5d). The result obeys Randles–Sevcik equation, indicating that these redox reactions occur under a diffusion control. From Figure S5, the electrochemical performance of the electrode in all

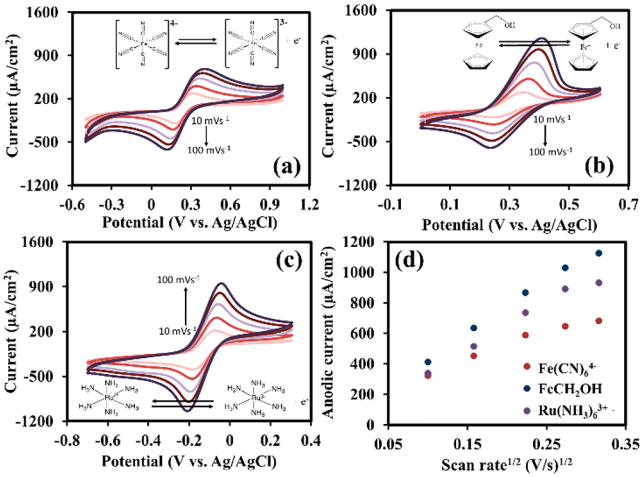

Figure 5. Cyclic voltammograms of ss-HSDNA/rGO_{ae} in 2 ng/mL AFB1 in 6 mM using different redox mediators: (a) $Fe(CN)_6^{4-}$, (b) $FcCH_2OH$, and (c) $Ru(NH_3)_6^{3+}$ in PBS (pH 7.4) as well as (d) the relationship between the square root of scan rate and the anodic current of ss-HSDNA/rGO_{ae} in three different redox mediators.

solutions is less than the theoretical current predicted by Randles–Sevcik equation resulting from the partially blocked active surface by biomolecules adsorbed on the active surface. In the case of $FcCH_2OH$, the anodic current response from the experiment is 21.3% lower than the predicted theoretical value. This redox mediator provides the closest current to the theoretical current as compared with other redox mediators. As discussed in the first section, for the $FcCH_2OH$ a neutral compound consisting of two cyclopentadienyl rings, the π cloud electron density on the flat aromatic ring may cause a noncovalent $\pi-\pi$ interaction from a cyclopentadienyl ring of the $FcCH_2OH$ molecule interacting with both a benzene ring on the graphene structure and the aromatic group in amino acid on the DNA structure leading to adsorption or preconcentration on the electrode surface.[33] Moreover, the cation molecule in both DNA and rGO_{ae} structures may be served as a cation/π interaction (i.e., N−H/π interaction).[34] On the other hand, the highly negative charge of the functional groups on the electrode electrostatically repulses the negatively charged $Fe(CN)_6^{4-}$. In the case of $Ru(NH_3)_6^{3+}$, the attractive force between the positively charged $Ru(NH_3)_6^{3+}$ and the negative charge of the electrode is dominant.

Effect of Hydrodynamic Diffusion. For the hydrodynamic study, the rate of chemical reaction depends on the rotation speed (ω) of a rotating disk electrode (RDE). Therefore, we use the EIS to observe the hydrodynamic effect by applying different rotation speeds. Note that, in order to avoid any interfering effect from fluctuating flow causing any bubble motion, the fluid stream is usually controlled under a laminar flow with a rotation speed range between $20 < \omega < 6000$ rpm.[35] At this speed range, it provides a high uniform accessibility of the reaction surface with a small aqueous diffusion layer thickness.

Figure 6 illustrates the EIS response of the ss-HSDNA/rGO_{ae} RDE electrode in 6 mM $FcCH_2OH$ in PBS (pH 7.4) containing 2 ng/mL AFB1 via applying the different rotation speeds (0–4000 rpm). By applying a small amplitude sinusoidal AC probed voltage as a function of frequency, the Nyquist plot presents the relation of imaginary impedance (Z'') and the real impedance component (Z'). At a static condition (0 rpm), a

DOI: 10.1021/acs.analchem.7b03329
Anal. Chem. 2017, 89, 13283–13289

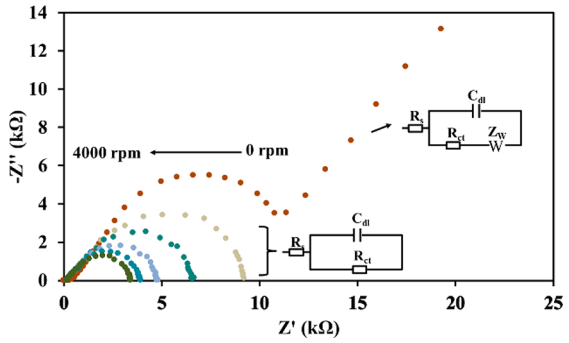

Figure 6. EIS of ss-HSDNA/rGO$_{ae}$ GC RDE in 2 ng/mL AFB1 in 6 mM FcCH$_2$OH in PBS (pH 7.4) at a potential of 0.32 V vs Ag/AgCl from 10 mHz to 10000 Hz at different rotation rates.

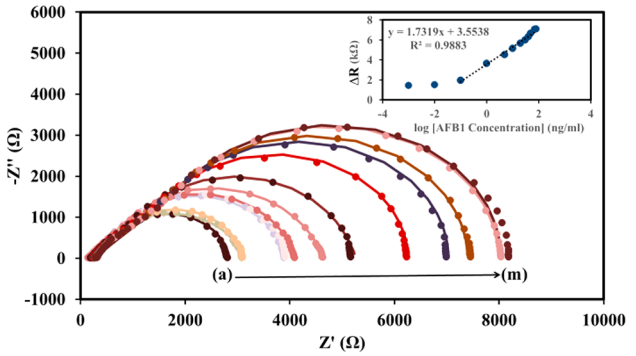

Figure 7. EIS of the ss-HSDNA/rGO$_{ae}$ GC RDE with different AFB1 concentrations; (a) 0, (b) 0.001, (c) 0.01, (d) 0.1, (e) 1.0, (f) 5.0, (g) 10.0, (h) 20.0, (i) 30.0, (j) 40.0, (k) 50.0, (l) 70.0, and (m) 80.0 ng/mL in 6 mM FcCH$_2$OH in PBS (pH 7.4). Inset image is a calibration curve (0.1 to 10.0 ng/mL) for AFB1 detection at a potential of 0.32 V vs Ag/AgCl from 10 mHz to 10000 Hz at a rotation speed 4000 rpm.

semicircle region at higher frequency indicates an electron transfer limit process, and a linear part at lower frequency corresponds to a diffusion process. The diffusion process can be defined by a parameter in term of Warburg impedance (Z_w) and this process is normally fitted in an equivalent circuit of Randles circuit, $R_s(C(R_{ct}Z_w)$.[36,37] The parameter detail can be seen in the Experimental Section. Here, a resistance of solution (R_s) has a similar value in every response from every applied speed which is fixed at 150 Ω. When we increased the rotation speeds up to 500, the linear part at the lower frequency disappeared meaning that the diffusion controlled process can be neglected. Then, the equivalent circuit is reduced to $R_s(CR_{ct})$. The diameter of the semicircle region relates to the amount of charge transfer resistance (R_{ct}). The R_{ct} value remarkably drops when the rotation speed rises as an expected result. This reduction of resistance results from the reduction of the film thicknesses, which are 3.2, 2.3, 1.6, 1.3, 1.1, and 0.92 μm at the rotation speeds of 500, 1000, 2000, 3000, 4000, and 6000 rpm, respectively (see calculation details in section 3.2 of the Supporting Information).

The EIS response at AFB1 concentrations was further recorded using the ss-HSDNA/rGO$_{ae}$ electrode placed in the PBS solution in the presence of 6 mM FcCH$_2$OH. By observing the change of the AFB1 concentration (0−10 ng/mL) under a static electrode (0 rpm), the obtained EIS profile does not show any significant difference, as shown in Figure S4a in the Supporting Information. This shows a limitation process of AFB1 diffusing from the bulk solution to the electrode surface. Therefore, the hydrodynamic diffusion was applied. Here we observed the response of two different rotating speeds (1000 and 4000 rpm), as shown in Figures S4b and 7, respectively. As the AFB1 concentration increases, the R_{ct} value increases, resulting from the increase of electron transfer resistance of the FcCH$_2$OH redox probe in the solution due to the insulator AFB1 molecule partly blocking and reducing active surfaces. This is good evidence of a capture process of AFB1 on the electrode surface.[38,39] The difference from this increasing R_{ct} represents R_{AFB1}. The ΔR_{ct} can be fitted as a linear relationship with the AFB1 concentration yielding a linear calibration plot with $R^2 > 0.96$ (see Table S3). The higher rotation speed (4000 rpm) provides the wider linear range for detection (1×10^{-10} to 7×10^{-8} g/mL) with the lower detection limit of 0.04 ng/mL based on three times standard deviation divided by the obtained calibration slope ((3SD$^-$)/slope). From the literature survey (Tables S2 and S3), the high-performance electrode for determining the AFB1 level mostly includes metallic materials for improving the electrocatalytic activity. By using our modified methodology, the sensing performance (see Table S3) provides a similar or even better performance as compared with other electrodes. The stability after used for 20 cycles is about 116.87% (Figure S7).

Sensitivity and Selectivity of AFB1 Detection and the Detection of AFB1 in Milk. To study the sensitivity and selectivity of the electrochemical sensor, other mycotoxins that can contaminate in human and animal such as aflatoxin B2 (AFB2), aflatoxin G2 (AFG2), and ochratoxin (OCH)[40] were tested. A total of 0.01 ng/mL of those samples was analyzed on the ss-HSDNA/rGO RDE in the PBS containing 6 mM FcCH$_2$OH in the presence of 0.01 ng/mL AFB1 using the EIS technique. The response was recorded at 0.32 V versus Ag/AgCl under a rotating speed of 4000 rpm. Again, 0.1, 1, and 10 ng/mL of those samples were observed in solutions with the presence of 0.1, 1, and 10 ng/mL AFB1, respectively (see Figure 8a). The response from the solution containing AFB2

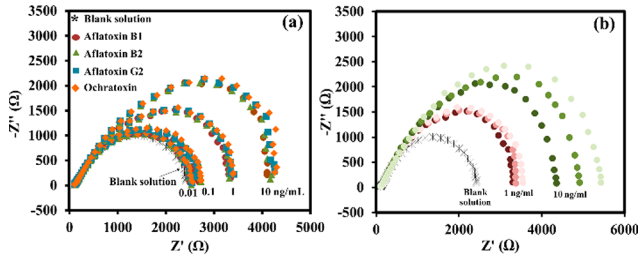

Figure 8. EIS of ss-HSDNA/rGO GC RDE: (a) sensitivity and selectivity to AFB1 as compared with aflatoxin B2, aflatoxin G2 and ochratoxin with four different concentrations (0.01, 0.1, 1.0, 10.0 ng/mL) and (b) real sample (UHT milk) injections at a potential of 0.32 V vs Ag/AgCl from 10 mHz to 10000 Hz in 6 mM FcCH$_2$OH in PBS (pH 7.4) at a rotation speed of 4000 rpm.

and OCH does not show any effect on the AFB1 response resulting from the lock and key process that has single base mismatched DNA with the AFB2 and OCH. The AFG2 has slightly perturbed the system providing the increase of the ΔR_{ct} about 4%. However, this interference is quite low and can be eliminated.

To demonstrate a practical application, the electrochemical sensor was applied to detect the AFB1 in UHT milk via an additional method. The EIS measurement (Figure 8b) was carried out using the UHT milk containing different AFB1

DOI: 10.1021/acs.analchem.7b03329
Anal. Chem. 2017, 89, 13283−13289

concentrations in 6 mM $FcCH_2OH$ in PBS (pH 7.4) at a rotation rate of 4000 rpm. Each concentration is analyzed three times. The percentage recovery was found in the range of 86–96%, as shown in Table S4 in the Supporting Information. This indicates that the proposed method is suitable for detecting AFB1 in the UHT milk.

CONCLUSION

A high sensitivity and selectivity capacitive biosensor for sensing aflatoxin B1 (AFB1) molecules on the ss-HSDA/rGO_{ae} electrode was demonstrated via considering two main effects including redox mediator and hydrodynamic diffusion. By observing the electrochemical response from three different charges of the redox mediator in the solution phase, the current respond magnitude of the ss-HSDA/rGO electrode is significantly dominated by the charge of the redox probe for which neutral $FcCH_2OH$ provides higher current than cationic $Ru(NH_3)_6^{3+}$ and anionic $Fe(CN)_6^{4-}$, respectively. The cationic $Ru(NH_3)_6^{3+}$ and anionic $Fe(CN)_6^{4-}$ molecules are dominant with the electrostatic force. In the case of neutral $FcCH_2OH$, which is the best mediator in this work, aromatic cyclopentadienyl rings on its structure can interact with an aromatic group (i.e., benzene rings on the graphene structure and aromatic groups on the amino acid) via $\pi-\pi$ interaction, and interact with cation molecules containing on DNA and rGO structures via cation/π interaction. The hydrodynamic diffusion was further considered using the EIS method with the ss-HSDA/rGO_{ae} modified on the RDE in the PBS solution containing $FcCH_2OH$ and AFB1 molecules. By applying different rotating speeds, the charge transfer resistance was reduced as increasing rotating speeds resulting in the lower detectable level for AFB1 quantification as compared with previous studies. This result indicates that a mass transport effect cannot be ignored in impedimetric sensors.

ASSOCIATED CONTENT

Supporting Information

The Supporting Information is available free of charge on the ACS Publications website at DOI: 10.1021/acs.analchem.7b03329.

Supporting figures including low magnification SEM image of rGO, FTIR of NHS and NHS/rGO, EIS of ss-HSDNA/rGO RDE at static condition, and 1000 rpm of various aflatoxin B1 concentrations, and an example of calculations such as film thickness and the detection limit. The table shows the previous studies of AFB1 detection (PDF)

AUTHOR INFORMATION

Corresponding Author

*Tel.: +66(0)33-01-4251. Fax: + 66(0)33-01-4445. E-mail: montree.s@vistec.ac.th.

ORCID

Montree Sawangphruk: 0000-0003-2769-4172

Author Contributions

M.S. conceived and designed this work and wrote the paper, and A.K. carried out the experiments.

Notes

The authors declare no competing financial interest.

ACKNOWLEDGMENTS

This work was financially supported by the Thailand Research Fund and Vidyasirimedhi Institute of Science and Technology (RSA5880043). Support from the Frontier Research Centre at VISTEC is also acknowledged.

REFERENCES

(1) Daly, S. J.; Keating, G. J.; Dillon, P. P.; Manning, B. M.; O'Kennedy, R.; Lee, H. A.; Morgan, M. R. A. *J. Agric. Food Chem.* **2000**, *48*, 5097–5104.

(2) Gilbert, J.; Anklam, E. *TrAC, Trends Anal. Chem.* **2002**, *21*, 468–486.

(3) Liu, J.-W.; Lu, C.-C.; Liu, B.-H.; Yu, F.-Y. *Food Control* **2016**, *59*, 700–707.

(4) Larou, E.; Yiakoumettis, I.; Kaltsas, G.; Petropoulos, A.; Skandamis, P.; Kintzios, S. *Food Control* **2013**, *29*, 208–212.

(5) Bonanni, A.; Pumera, M. *Electrochem. Commun.* **2013**, *26*, 52–54.

(6) Masoomi, L.; Sadeghi, O.; Banitaba, M. H.; Shahrjerdi, A.; Davarani, S. S. H. *Sens. Actuators, B* **2013**, *177*, 1122–1127.

(7) Banitaba, M. H.; Davarani, S. S. H.; Mehdinia, A. *Anal. Biochem.* **2011**, *411*, 218–222.

(8) Dinçkaya, E.; Kınık, Ö.; Sezgintürk, M. K.; Altuğ, Ç.; Akkoca, A. *Biosens. Bioelectron.* **2011**, *26*, 3806–3811.

(9) Sirisinudomkit, P.; Iamprasertkun, P.; Krittayavathananon, A.; Pettong, T.; Dittanet, P.; Sawangphruk, M. *Sci. Rep.* **2017**, *7*, 9.

(10) Lu, L.; Guo, L.; Kang, T.; Cheng, S. *Microchim. Acta* **2017**, *184*, 2949–2957.

(11) Patil, A. V.; Fernandes, F. B.; Bueno, P. R.; Davis, J. J. *Bioanalysis* **2015**, *7*, 725–742.

(12) Patolsky, F.; Lichtenstein, A.; Willner, I. *Angew. Chem., Int. Ed.* **2000**, *39*, 940–943.

(13) Sanguansak, Y.; Srimuk, P.; Krittayavathananon, A.; Luanwuthi, S.; Chinvipas, N.; Chiochan, P.; Khuntilo, J.; Klunbud, P.; Mungcharoen, T.; Sawangphruk, M. *Carbon* **2014**, *68*, 662–669.

(14) Wang, C.; de Jong, E.; Sjollema, K. A.; Zuhorn, I. S. *Sci. Rep.* **2016**, *6*, 21436.

(15) Ito, Y.; Qiu, H. J.; Fujita, T.; Tanabe, Y.; Tanigaki, K.; Chen, M. *Adv. Mater.* **2014**, *26*, 4145–4150.

(16) Naveen, M. H.; Gurudatt, N. G.; Noh, H.-B.; Shim, Y.-B. *Adv. Funct. Mater.* **2016**, *26*, 1590–1601.

(17) Mamidi, S. S.; Meas, B.; Farhat, T. R. *Anal. Chem.* **2008**, *80*, 8109–8114.

(18) Masa, J.; Batchelor-McAuley, C.; Schuhmann, W.; Compton, R. G. *Nano Res.* **2014**, *7*, 71–78.

(19) Huskinson, B.; Marshak, M. P.; Suh, C.; Er, S.; Gerhardt, M. R.; Galvin, C. J.; Chen, X.; Aspuru-Guzik, A.; Gordon, R. G.; Aziz, M. J. *Nature* **2014**, *505*, 195–198.

(20) Hummers, W. S.; Offeman, R. E. *J. Am. Chem. Soc.* **1958**, *80*, 1339–1339.

(21) Sawangphruk, M.; Srimuk, P.; Chiochan, P.; Sangsri, T.; Siwayaprahm, P. *Carbon* **2012**, *50*, 5156–5161.

(22) Pettong, T.; Iamprasertkun, P.; Krittayavathananon, A.; Sukha, P.; Sirisinudomkit, P.; Seubsai, A.; Chareonpanich, M.; Kongkachuichay, P.; Limtrakul, J.; Sawangphruk, M. *ACS Appl. Mater. Interfaces* **2016**, *8*, 34045–34053.

(23) Krittayavathananon, A.; Iamprasertkun, P.; Sawangphruk, M. *Carbon* **2016**, *109*, 314–320.

(24) Suni, I. I. *TrAC, Trends Anal. Chem.* **2008**, *27*, 604–611.

(25) Ren, H.; Shi, X.; Zhu, J.; Zhang, Y.; Bi, Y.; Zhang, L. *J. Mater. Sci.* **2016**, *51*, 6419–6427.

(26) Wang, C.; Jia, X.-M.; Jiang, C.; Zhuang, G.-N.; Yan, Q.; Xiao, S.-J. *Analyst* **2012**, *137*, 4539–4545.

(27) Saito, S.; Silva, G.; Santos, R. X.; Gosmann, G.; Pungartnik, C.; Brendel, M. *Int. J. Mol. Sci.* **2012**, *13*, 2846–2862.

(28) Bocking, T.; Kilian, K. A.; Reece, P. J.; Gaus, K.; Gal, M.; Gooding, J. J. *Soft Matter* **2012**, *8*, 360–366.

(29) Gao, W.; Feng, B.; Ni, Y.; Yang, Y.; Lu, X.; Weng, J. *Appl. Surf. Sci.* **2010**, *257*, 538–546.

DOI: 10.1021/acs.analchem.7b03329
Anal. Chem. 2017, 89, 13283–13289

(30) Zhang, J.; Dai, L. *ACS Catal.* **2015**, *5*, 7244−7253.
(31) Feng, L.; Chen, Y.; Ren, J.; Qu, X. *Biomaterials* **2011**, *32*, 2930−2937.
(32) Singh, C.; Srivastava, S.; Ali, M. A.; Gupta, T. K.; Sumana, G.; Srivastava, A.; Mathur, R. B.; Malhotra, B. D. *Sens. Actuators, B* **2013**, *185*, 258−264.
(33) Lanzarotti, E.; Biekofsky, R. R.; Estrin, D. A.; Marti, M. A.; Turjanski, A. G. *J. Chem. Inf. Model.* **2011**, *51*, 1623−1633.
(34) Forbes, C. R.; Sinha, S. K.; Ganguly, H. K.; Bai, S.; Yap, G. P. A.; Patel, S.; Zondlo, N. J. *J. Am. Chem. Soc.* **2017**, *139*, 1842−1855.
(35) Adams, R. N. *Electrochemistry at Solid Electrodes*; Dekker, 1969.
(36) Bonanni, A.; Loo, A. H.; Pumera, M. *TrAC, Trends Anal. Chem.* **2012**, *37*, 12−21.
(37) Bonanni, A.; Pumera, M. *ACS Nano* **2011**, *5*, 2356−2361.
(38) Yu, L.; Zhang, Y.; Hu, C.; Wu, H.; Yang, Y.; Huang, C.; Jia, N. *Food Chem.* **2015**, *176*, 22−26.
(39) Xu, H.; Wang, L.; Ye, H.; Yu, L.; Zhu, X.; Lin, Z.; Wu, G.; Li, X.; Liu, X.; Chen, G. *Chem. Commun.* **2012**, *48*, 6390−6392.
(40) Weidenbörner, M. *Natural Mycotoxin Contamination in Humans and Animals*; Springer International Publishing, 2015.

DOI: 10.1021/acs.analchem.7b03329
Anal. Chem. 2017, 89, 13283−13289